J. Fluid Mech. (1975), *vol.* 70, *part* 1, *pp.* 1–15
Printed in Great Britain

Statistical characteristics of a turbulent jet

By M. M. RIBEIRO AND J. H. WHITELAW
Department of Mechanical Engineering, Imperial College, London

(Received 1 July 1974 and in revised form 12 December 1974)

Velocity probability distributions and autocorrelation functions were measured in the self-preserving region of a round free jet at 57 diameters. On-line digital-sampling procedures were used to interpret the signals from a crossed hot-wire probe. Particular attention was paid to the probabilities of the axial and radial velocity components and of the angle between them at radial locations corresponding to the centre-line and the location of maximum shear stress and at an edge location $r/x = 0{\cdot}087$.

The results show, for example, that the probability of the axial velocity on the centre-line is slightly non-Gaussian and that, in general, the observed deviations of the probabilities of u depend upon the difference in behaviour of the corresponding distributions for positive and negative v; outward transport (positive v) is associated with near-Gaussian u distributions whereas inward transport (negative v) is associated with skewed u distributions. The probability of the fluctuating vector (u, v) becomes more asymmetric with increasing radius with the dominant direction corresponding to positive $\overline{uv}$. The measured auto- and cross-correlations are shown to be largely independent of radius.

1. Introduction

The turbulence properties of self-preserving round jets have previously been considered by, for example, Gibson (1963) and Wygnanski & Fiedler (1969). The information presented in these papers is extensive but does not include measurements of probability density distributions although, as observed by Gupta & Kaplan (1972) and Antonia (1972) in their investigations of wall boundary layers, such measurements can provide additional and useful information on the turbulent flow.

The present paper establishes that the jet flow under consideration possesses profiles of mean velocity and Reynolds stresses at 57 diameters downstream which accord with expectations based on previous investigations. It then presents autocorrelations and velocity probability distributions measured in the self-preserving region. Particular attention is paid to the probabilities of the axial and radial velocity components and of the angle between them and relevant physical information and implications are examined.

The measurements were obtained using on-line digital sampling of the signals from a crossed hot-wire probe. The sampling and averaging techniques did not incorporate conditional sampling procedures and the averages include, therefore,

contributions from signals obtained at times when the velocity was turbulent and non-turbulent. The principal radial measuring stations corresponded to the centre-line, the location of maximum Reynolds shear stress and the location where the mean velocity was half the centre-line value.

The paper is divided into three sections, which describe the apparatus and its operation, present and discuss the results and offer concluding remarks. The apparatus consisted of a jet, hot-wire instrumentation and a data-processing computer; these, and the associated signal-processing procedure, are described in the next section. The following section presents measured values of the mean velocity and Reynolds stresses and demonstrates that they are in agreement with the measurements of previous authors; probability distributions and auto-correlations are then presented and discussed. The concluding remarks relate the present measurements to previous measurements and present general conclusions.

2. Experimental apparatus and procedure

2.1. *Jet arrangement*

The jet arrangement used for the present investigation was similar to that previously used by Rodi (1972). It consisted of an orifice 12·9 mm in diameter located in one surface of a $1{\cdot}06 \times 0{\cdot}52 \times 0{\cdot}52$ m plenum chamber which contained two screens and two sections of honeycomb. A fan delivered air through an electrostatic filter to another plenum chamber, where pressure pulsations were damped, before passing it to the plenum chamber containing the orifice. The average jet orifice velocity for the present measurements was 83·4 m/s, corresponding to a Reynolds number of $7{\cdot}1 \times 10^4$.

A screen cage $2 \times 2 \times 5$ m long with a $\frac{1}{16}$ in. mesh surrounded the jet flow on three sides and minimized the possible influence of draughts. The hot-wire probe holder was supported on a cathetometer which, in turn, was secured to a small milling table: this arrangement allowed precise movement of the probe holder in three orthogonal directions.

2.2. *Hot-wire and data-processing equipment*

A line diagram of the signal-processing equipment is presented in figure 1 and indicates that the signals from a crossed hot-wire probe (DISA 55A32) were passed to linearizers (DISA 55D10) through constant-temperature anemometers (DISA 55D01). The voltage signals from the linearizers were supplied to sample-and-hold units (Burr Brown SHM 40) which, in turn, were controlled and sampled by a small computer (Digital PDP8E). This sampling arrangement permitted samples to be obtained at a frequency of 20 kHz.

2.3. *Experimental procedures*

Calibration. The anemometers were linearized and calibrated with the probe in the potential core of a calibration jet, using digital techniques. The turbulence intensity was less than 2% and the velocity was continuously variable. The

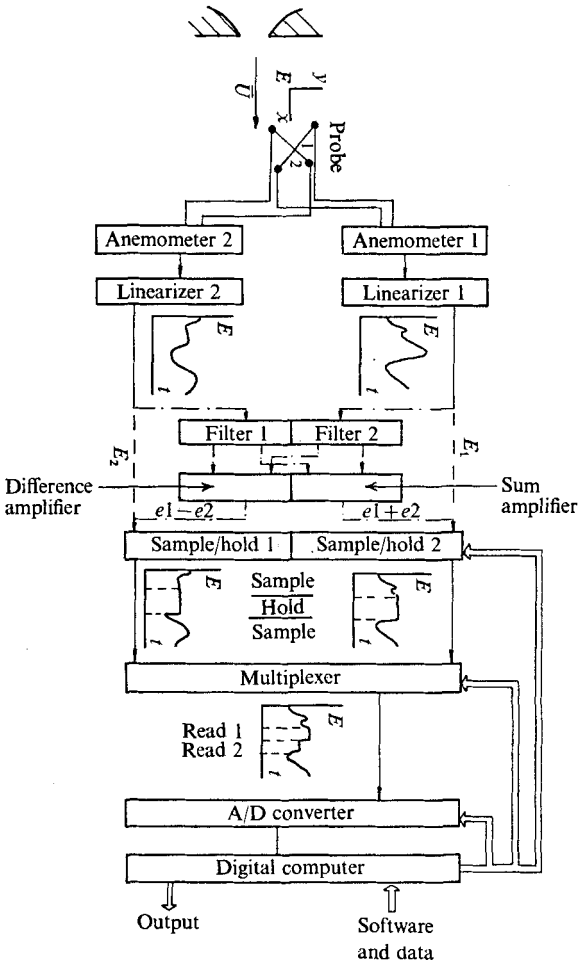

FIGURE 1. Diagram of data-acquisition arrangement. ——, – – –, route for mean velocity andReynoldsstresses; ——, – · – · –, route for probability density distributions and time correlations.

calibration arrangement allowed rotation of the probe around a fixed point on the axis of the jet one nozzle diameter downstream from the exit.

The output E from the linearizer was compared with the velocity U measured by a Pitot tube placed in the same axial plane as the hot wire but 5 mm away. Signals from the linearizer and pressure transducer were input to the A/D interface. The velocity was determined from the Pitot tube and the ratio between the velocity and linearizer output calculated for several values of the velocity between 5 and 35 m/s. Exponent and zero settings of the linearizer were adopted until a satisfactory linearization was achieved; typical values obtained are summarized in table 1. After linearization, the relationship between E and U was

$$E = SU_{\text{eff}}, \tag{1}$$

where $U_{\text{eff}} = f(\alpha)\, U$ with $f(\alpha)$ dependent only on the yaw angle α.

Velocity, U (m/s)	E (from linearizer)	Ratio, E/U
35·002	3·6915	0·1055
32·324	3·4084	0·1055
27·113	2·8600	0·1055
22·587	2·3847	0·1056
18·848	1·9894	0·1056
15·487	1·6270	0·1051
12·167	1·2747	0·1048
8·8887	0·9370	0·1054
5·5307	0·5858	0·1059

TABLE 1

With the cosine law of Champagne & Sleicher (1967) the above relationship becomes

$$E^2 = S^2U^2(\cos^2\alpha + k^2\sin^2\alpha). \tag{2}$$

Thus the calibration determined both the calibration constant S and the yaw factor k (typical values of k were 0·1 and 0·17); for each velocity, two values of α are needed to determine S and k. Because the cosine law only holds for a limited range of α, angles were chosen near the working values of α for the flow situation (30°, 45° and 60°). For example, for $\alpha_1 = 30°$ and $\alpha_2 = 45°$, S^2 and k^2 become

$$S^2 = \frac{2E^2(30) - E^2(45)}{U^2}, \quad k^2 = \frac{3E^2(45) - 2E^2(30)}{-E^2(45) + 2E^2(30)}.$$

Calibration was carried out for each wire, and by suitable adjustment of the gain of the linearizers, the values of S were made to coincide.

The response from the two anemometers was tested with the axis of the probe aligned with the flow direction in the calibration rig. The signals from both linearizers were input to the A/D interface and the multiplexer switched between the two channels, at a rate of 1 ms/channel, by suitable software. At the same time, the velocity was continuously changed. The output from the multiplexer was a.c. coupled and monitored in an oscilloscope set at 0·02 V/division. Any imbalance between the channels would have appeared as a square wave form on the screen. No square wave forms were observed.

Mean velocity and Reynolds stresses. A schematic diagram of the data acquisition is shown in figure 1. Signals from the cross-wire probe, with its axis aligned with the mean flow direction, were linearized and input to the A/D interface through the sample-and-hold circuits. With the wires in the plane Oxr and with the axis of the probe aligned with the mean flow direction, linearized signals are related to the velocity field (Champagne & Sleicher 1967) by the following equations:

$$\overline{U} = \frac{1}{2\frac{1}{2}S(1 + \frac{1}{2}k^2 - \frac{1}{8}k^4)}(\overline{E}_1 + \overline{E}_2), \tag{3}$$

$$\frac{\overline{u^2}}{\overline{U}^2} = \frac{1}{4}\overline{\left(\frac{E_1}{\overline{E}_1} + \frac{E_2}{\overline{E}_2} - 2\right)^2} = \frac{1}{4}\left(\frac{\overline{E_1^2}}{\overline{E}_1^2} + \frac{\overline{E_2^2}}{\overline{E}_2^2} + 2\frac{\overline{E_1E_2}}{\overline{E}_1\overline{E}_2}\right) - 1, \tag{4}$$

$$\frac{\overline{v^2}}{\overline{U}^2} = \frac{1}{4}\left(\frac{1+k^2}{1-3k^2+4k^4}\right)\left(\frac{\overline{E_1}-\overline{E_2}}{\overline{E}_1-\overline{E}_2}\right)^2 = \frac{1}{4}\left(\frac{1+k^2}{1-3k^2+4k^4}\right)\left(\frac{\overline{E_1^2}}{\overline{E}_1^2}+\frac{\overline{E_2^2}}{\overline{E}_2^2}-2\frac{\overline{E_1E_2}}{\overline{E}_1\overline{E}_2}\right), \quad (5)$$

$$\frac{\overline{uv}}{\overline{U}^2} = \frac{1}{4}\left(\frac{1+k^2}{1-k^2}\right)\left(\frac{\overline{E_1^2}}{\overline{E}_1^2}-\frac{\overline{E_2^2}}{\overline{E}_2^2}\right), \quad (6)$$

where E represents a linearized signal, S the calibration constant and k the yaw factor; the subscripts 1 and 2 refer to wires 1 and 2 and overbars denote time averages. $\overline{U}$ represents the mean velocity, $\overline{u^2}$ and $\overline{v^2}$ are the Reynolds normal stresses in the axial (x) and radial (r) directions and $\overline{uv}$ is the Reynolds shear stress in the plane Oxr.

Knowledge of $\overline{E}_1$, $\overline{E}_2$, $\overline{E_1E_2}$, $\overline{E_1^2}$ and $\overline{E_2^2}$ is sufficient to determine the mean velocity and the three Reynolds stresses in the plane Oxr. Values of $E_1(t)$ and $E_2(t)$ were sampled in the way described in the last paragraph. Basically, loops of 384 samples of E_1 and E_2 were repeated 200–400 times, according to the flow characteristics at the probe location. At the end of each loop, mean values for the five quantities were calculated for the loop, and used to update the corresponding total mean. Finally, the mean velocity and Reynolds stresses were calculated according to the above set of equations.

Time correlation. Time correlations were obtained by a sampling process similar to that described in the last paragraph; sets of 192 pairs (u, v) for each instant were stored sequentially with u preceding v and contiguous pairs corresponding to a unit time delay. To obtain the desired correlation, values were cross-multiplied and each pair was used a number of times equal to the total number of discrete points constituting the correlation. After each set of 192 pairs was complete and the values of the correlation for the different delays had been calculated, these values were used to update the corresponding means. Execution of the program ended when a new set did not influence any of the means by more than 1 %.

In order to determine the unit time delay, a dummy run was made and the period of the digital pulse controlling the logic commanding the A/D converter was measured. Different unit time delays were obtained by execution of a do-nothing set of instructions a different number of times. The minimum elemental time step was 64 μs and could be increased indefinitely by steps of 1·2 μs.

Single probability density distributions. For an ideal X-wire array aligned with the flow direction and with the wires in plane Oxy, Champagne & Sleicher (1967) indicate that

$$u = \frac{1}{2^{\frac{1}{2}}S(1+\frac{1}{2}k^2-\frac{1}{8}k^4)}(e_1+e_2) = \alpha(e_1+e_2),$$

$$v = \frac{1}{2^{\frac{1}{2}}S}\left(\frac{1+k^2}{(1-3k^2+4k^4)}\right)^{\frac{1}{2}}\frac{1}{1+\frac{1}{2}k^2-\frac{1}{8}k^4}(e_1-e_2) = \beta(e_1-e_2),$$

where S is the calibration constant, k the yaw factor and e_1 and e_2 the a.c. components of E_1 and E_2 (linearized outputs from wires that react dominantly to uv positive and negative, respectively); u and v are the velocity fluctuations in the axial and radial directions.

Thus E_1 and E_2 were input to high-pass filters, added and subtracted to yield voltages proportional to u and v. Each voltage was applied to the A/D interface and sampled. The voltage range was divided into 128 equally spaced intervals and a 24 bit binary word was associated with each interval. For each value sampled, the corresponding word was determined and its value increased by one. The total number of samples was 2×8^7 (4194304). The histogram obtained was afterwards normalized to have unit area and higher-order moments were calculated.

Specific problems were the following.

(i) Non-uniform size of voltage intervals: this was cured by obtaining the probability density distribution of a ramp; weight factors for each interval were determined from the distribution.

(ii) High frequencies present in the signal, implying voltage changes during the process of A/D conversion, were cured by the insertion of a sample-and-hold circuit between the multiplexer and the A/D converter. Aperture times were reduced from 24 μs to 100 ns.

(iii) Dominant frequencies eventually present in the signal jointly with a single frequency of sampling could distort the results; this problem was cured by the insertion of a random time delay between two consecutive readings.

Joint probability density distributions. Basically the process was the same as for the last case, but the two signals proportional to u and v respectively were first 'held' at the same instant, followed by the A/D conversion and storage of each of these. Afterwards the 'sample' mode was restored.

The voltage range for both signals was divided into one array of 32×32 equally spaced intervals, each associated with a 24 bit binary word whose contents were increased by one each time the pair of voltages was inside the corresponding interval. The number of samples was 2×8^7; the histogram obtained was further processed in a CDC 6400 to yield the joint probability distribution and related quantities.

Specific problems were the same as for the last case and were solved in similar ways.

3. Measurements and discussion

3.1. *Preliminary remarks*

The present jet had previously been used by Rodi (1972), who reported extensive measurements of the mean velocity and turbulent quantities in the self-preserving region. All the discussion that follows refers to the measurements at three radial locations 57 diameters downstream of the inlet, for which the values of the mean velocity, turbulence intensities and skewness and flatness factors are shown in table 2.

3.2. *Probability distributions*

Probability density distributions have been measured for u, v, u/v and (u, v) at radial locations corresponding to the centre-line and the position of maximum turbulent shear stress ($r/x = 0{\cdot}056$) and at the location where the mean velocity

r/x	$U/U_{\mathbb{C}}$	$\overline{u^2}/U$	$\overline{v^2}/U$	$\overline{u^3}/(\overline{u^2})^{\frac{3}{2}}$	$\overline{v^3}/(\overline{v^2})^{\frac{3}{2}}$	$\overline{u^4}/(\overline{u^2})^2$	$\overline{v^4}/(\overline{v^2})^2$
0·000	1	0·244	0·193	−0·01	−0·01	2·98	2·98
0·056	0·749	0·325	0·232	0·22	0·38	3·06	3·28
0·087	0·503	0·457	0·310	0·46	0·61	3·45	3·90

TABLE 2

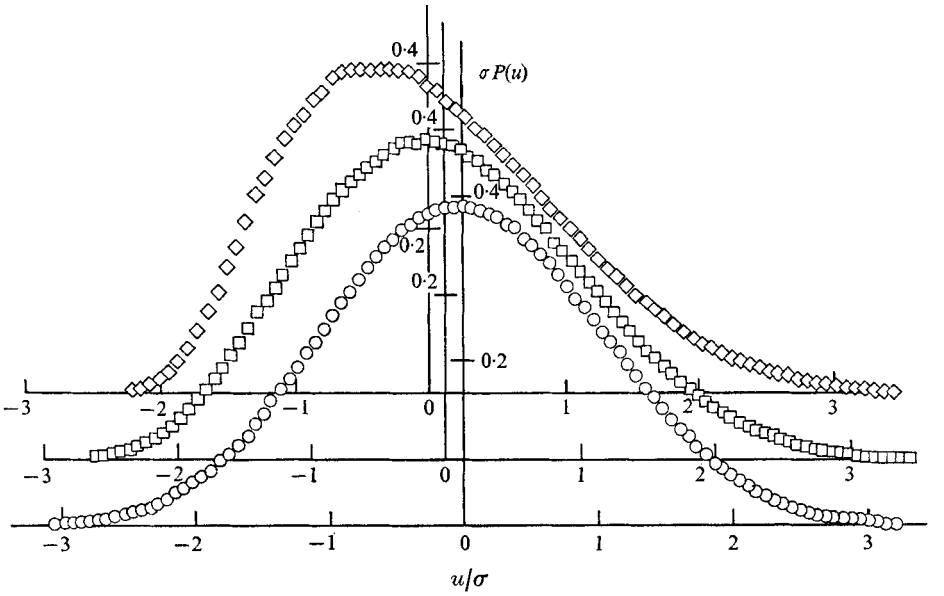

FIGURE 2. Probability density distributions of the u component of the fluctuating velocity at $x/D = 57$. ○, $r/x = 0{\cdot}000$; □, $r/x = 0{\cdot}056$; ◇, $r/x = 0{\cdot}087$.

is half the centre-line value ($r/x = 0{\cdot}087$). The measurements correspond to the cross-sectional plane at $x/D = 57$.

Figure 2 presents the probability distribution $P(u)$ of u and indicates nearly symmetrical behaviour on the centre-line: the existence of a small asymmetry is confirmed by the distribution of (u, v) which is presented later in this section. At the higher values of r/x there is a positive skewness with a flat region for u/σ between -1 and $0{\cdot}1$; the cause of this behaviour is revealed in figure 3, where the probability distributions of u at the three radial locations have been separated according to the sign of v. On the centre-line, by virtue of the symmetry, no dependence on the sign of v occurs, but away from the centre-line, the u distributions depend strongly on the sign of v: for positive v, the u distributions are nearly symmetrical with the mean value shifted towards the high velocity region ($0{\cdot}29\sigma$ for $r/x = 0{\cdot}056$ and $0{\cdot}34\sigma$ for $r/x = 0{\cdot}087$), whereas for negative v, distributions of u are positively skewed ($0{\cdot}31$ at $r/x = 0{\cdot}056$ and $0{\cdot}57$ for $r/x = 0{\cdot}087$) and their most probable values are less by $0{\cdot}6\sigma$ than the mean values of the overall distribution. The occurrence of differently located distributions enables the determination of a length scale of the mixing-length type, by relating the

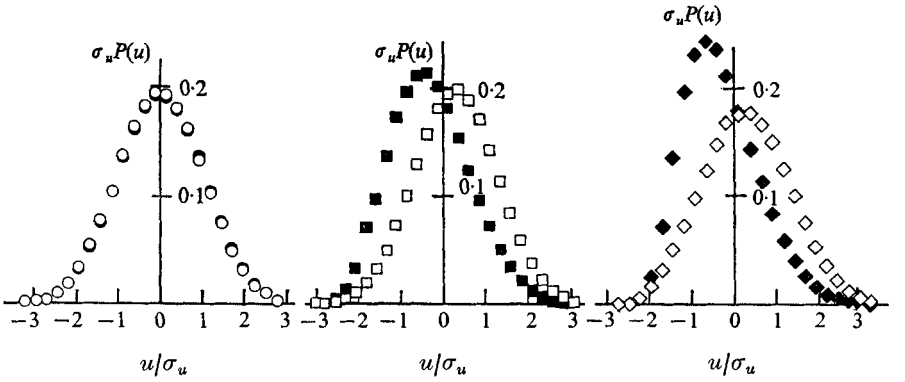

FIGURE 3. Probability density distributions of the u component of the fluctuating velocity divided according to the sign of v, at $x/D = 57$. Open symbols, $v > 0$; solid symbols, $v < 0$. r/x values for symbols as in figure 2.

characteristic velocity, i.e. the mean value of u for positive and negative v, of the two distributions to the local mean velocity: if no appreciable dissipation of x momentum occurs inside the region that affects the local velocity, it is given by

$$L = \frac{\Delta U}{\partial U/\partial r}$$

(ΔU being half the difference between the characteristic velocities of the separate distributions for $v \gtrless 0$).

When L is normalized by $r_{\frac{1}{2}}$, and the other quantities by measured quantities, the above expression becomes

$$\frac{L}{r_{\frac{1}{2}}} = \frac{x}{r_{\frac{1}{2}}} \frac{[(\mu_u)_{v>0} - (\mu_u)_{v<0}]\,\sigma_u/U_{\mathfrak{C}}}{\partial(U/U_{\mathfrak{C}})/\partial(r/x)}.$$

$(\mu_u)_{v \lessgtr 0}$ are the mean values of the u distribution when $v \gtrless 0$; σ_u is the standard deviation of $P(u)$. Length scales were obtained with the aid of the data in tables 2 and 3 and figure 2 and had values of 0·123 for $r/x = 0{\cdot}056$ and 0·122 for $r/x = 0{\cdot}087$.

It is interesting to note that, even for a nearly Gaussian distribution of u, when v is positive (figure 3) its contribution to the turbulent shear stress is significant and stems from the fact that its mean value is shifted from the overall mean value.

Figure 4 presents the probability density distributions of v at the same three radial locations. A symmetrical distribution occurs at the centre-line while as r/x increases a positive skewness develops. Away from the centre-line, the tails of the distribution indicate higher flatness factors; the most probable values appear to be less displaced from the mean than for the corresponding u distributions and the distributions seem far from Gaussian. However, in figure 5, where the v distributions are split according to the sign of u, it can be seen that the individual distributions are much closer to Gaussian than figure 2 would suggest. The distributions of v at the centre-line are particularly interesting in

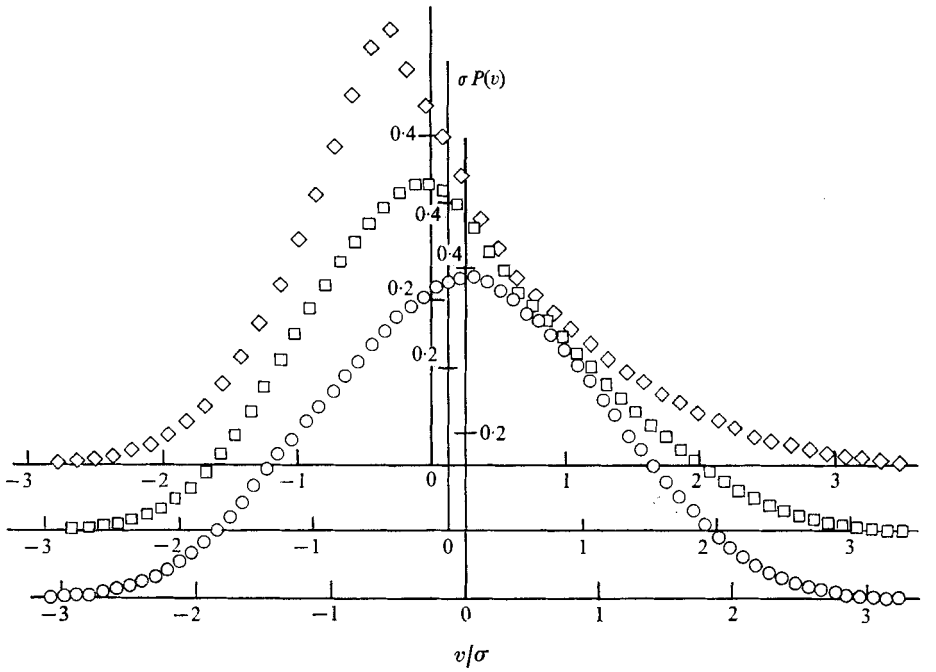

FIGURE 4. Probability density distributions of the v component of the fluctuating velocity at $x/D = 57$. Symbols as in figure 2.

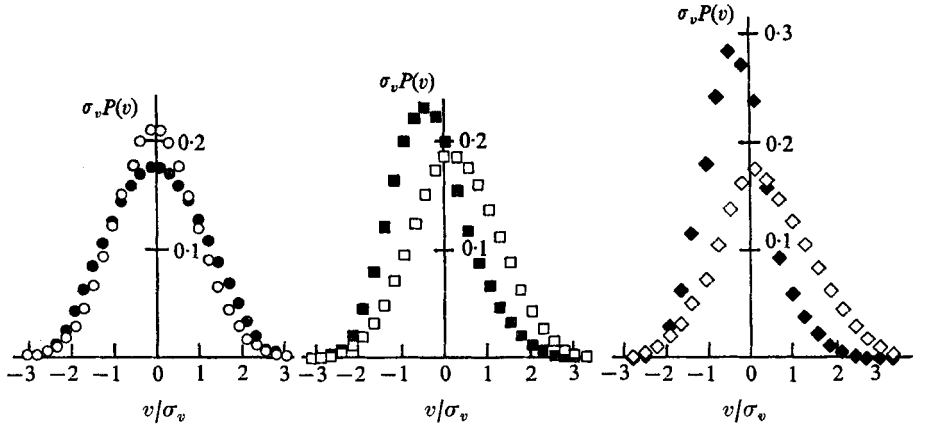

FIGURE 5. Probability density distributions of the v component of the fluctuating velocity divided according to the sign of u, at $x/D = 57$. Open symbols, $u > 0$; solid symbols, $u < 0$. r/x values for symbols as in figure 2.

that, unlike those of u, they are symmetrical but have different standard deviations with higher probabilities for high $|v|$ corresponding to negative u (see table 3 for the ratios of standard deviations for both distributions). This is consistent with the impression that high values of $|v|$ must correspond to larger distances of travel and that the associated eddies originate far from the centre-line; it also emphasizes the asymmetrical behaviour of u at the centre-line.

u_i	r/x	$(\sigma_{u_i})_{u_j<0}/(\sigma_{u_i})_{u_j>0}$	$[(\mu_{u_i})_{u_j>0}-(\mu_{u_i})_{u_j<0}]/\sigma_{u_i}$
u	0	1·02†	0·02‡
	0·056	0·95	0·29
	0·087	0·86	0·31
v	0	1·13	0·02‡
	0·056	0·88	0·29
	0·087	0·72	0·31

† This number should be 1·0 by virtue of symmetry around the x axis at the centre-line.
‡ These values should be zero for the same reasons.

TABLE 3

Table 3 shows a comparison of the u and v distributions: the difference between the mean values for positive and negative velocities is the same for u and v at each radial location. The ratio of the standard deviations of the negative and positive distributions decreases when r/x increases, and changes at a faster rate for u than for v.

Table 4 shows quantitatively the deviation of the distributions from Gaussian behaviour, by comparing the experimental results with sixth-order Gram–Charlier expansions (Lumley 1970, p. 39; Frenkiel & Klebanoff 1973):

$$f_{GC}(u_i) = \frac{1}{(2\pi)^{\frac{1}{2}}} \exp(-\tfrac{1}{2}u_i^2) \sum_{j=0}^{6} A_j H_j(u_i),$$

with

$$A_j = \frac{1}{j!}\int_{-\infty}^{\infty} H_j(u_i) f(u_i)\, du_i$$

and

$$H_j(u_i) = \exp(\tfrac{1}{2}u_i^2)\frac{\partial^j}{\partial u_i^j}\exp(-\tfrac{1}{2}u_i^2).$$

It shows that, generally, the conditional distributions are more closely approximated than the overall distributions; this is mainly true for u, thus emphasizing the difference between the behaviour associated with transport towards the centre-line and that for transport towards the edge.

Thus a general conclusion is that the deviation of the probability density distributions of u and v from Gaussian behaviour is largely dependent on the difference in behaviour of the corresponding distributions for positive and negative v. Positive-v distributions are associated with a nearly Gaussian behaviour for u, whereas negative-v distributions (inwards transport) may be coupled with positively skewed distributions for u.

Figure 6 presents probability density distributions of the direction of the fluctuating vector (u, v) at the three radial locations under examination. The centre-line distribution is symmetrical about the axial direction; it shows maxima close to the radial direction and a minimum in the axial direction with a ratio of approximately 2·7. This implies that the probability of $|v|$ being greater than $|u|$ is higher than the reverse. However, u^2 is larger than v^2; thus axial fluctuations are larger than radial fluctuations but less probable (this is consistent with the fact that energy spectra of v contain less energy than those of u but have higher

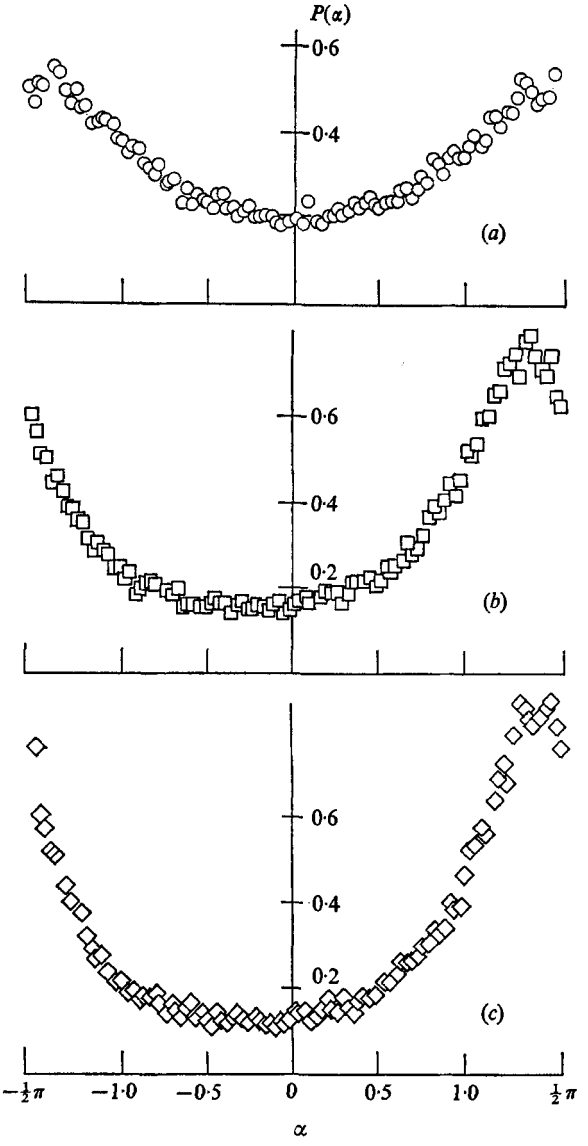

FIGURE 6. Probability density distributions of the direction of the fluctuating vector (u, v) at $x/D = 57$. Symbols as in figure 2.

density in the high frequency region). As r/x increases, the asymmetry of the distributions increases with the dominant directions shifting towards the first and third quadrants (uv positive). The two maxima occur close to each other because, as a result of an anticlockwise shift, the maximum in the fourth quadrant moves to the first quadrant. The ratio between the maximum and the minimum increases to 5·2 at $r/x = 0{\cdot}056$ and 7·8 at $r/x = 0{\cdot}087$ and indicates a corresponding increase in the time for which $|v| > |u|$.

Distribution	Condition	r/x	A_3	A_4	A_5	A_6	Maximum deviation in region $(-\sigma, +\sigma)$†
u	—	0	−0·012	0·0066	0·0008	−0·0004	1%
	$v > 0$		0·004	0·0058	0·0000	−0·0004	0·3%
	$v < 0$		0·000	0·0080	0·0000	−0·0004	0·3%
	—	0·056	−0·045	0·0082	0·0034	−0·0011	0·3%
	$v > 0$		0·004	0·0040	−0·0004	0·0002	0·8%
	$v < 0$		−0·051	0·0039	0·0031	−0·0010	1%
	—	0·087	−0·093	−0·0021	0·0063	−0·0023	5%
	$v > 0$		0·022	0·0106	0·0004	−0·0008	1·5%
	$v < 0$		−0·096	−0·0087	0·0038	0·0026	3%
v	—	0	−0·002	0·0114	0·0000	−0·0008	2·5%
	$u > 0$		−0·001	0·0042	−0·0002	0·0000	0·4%
	$u < 0$		−0·010	0·0211	0·0015	−0·0021	0·3%
	—	0·056	−0·054	0·0022	0·0060	−0·0001	5%
	$u > 0$		0·002	0·0068	0·0007	0·0000	0·3%
	$u < 0$		−0·055	0·0013	0·0048	0·0004	5%
	—	0·087	−0·108	−0·0279	0·0050	0·0002	10%
	$u > 0$		−0·017	0·0035	0·0034	0·0005	0·5%
	$u < 0$		−0·048	−0·0110	0·0005	0·0015	6%

† Owing to the nature of the approximation, values that exhibit higher deviations are located in regions where $u_i/\sigma < 1$.

TABLE 4

Figure 7 shows joint probability distributions of u and v as lines of constant density. These functions are defined by the equations

$$P(u,v)\,du\,dv = P\{u^* \in [u, u+du], v^* \in [v, v+dv]\},$$

$$\int_{-\infty}^{+\infty} d(u/\sigma_u) \int_{-\infty}^{+\infty} P(u,v)\,d(v/\sigma_v) = 1,$$

with σ_u and σ_v representing the standard deviations of $P_u(u)$ and $P_v(v)$, the probability density distributions of u and v. At the centre-line, the isodensity lines are symmetrical about $u = 0$, and thus the zero shear stress at this location stems from the particular location of the axis and not independence of u and v. For high values of $-u$, the v distribution exhibits a small flatness, which increases with u. The high values of v tend to coexist with negative values of u, i.e. the probability of occurrence of $|v/\sigma_v| = 2$ is greater for $u/\sigma_u = -1$ than for $u = 0$; thus high deficits in the axial mean velocity are coupled with strong radial fluctuations.

At $r/x = 0{\cdot}056$ and $0{\cdot}087$, the above tendency is reversed and high positive values of u coexist with high positive values of v. There appears to be no counterpart in the inward turbulent transport and thus it is nearly Gaussian travel towards the edge of the jet, rather than a skewed behaviour related to inward x-momentum transport, which is the main contributor to the Reynolds shear

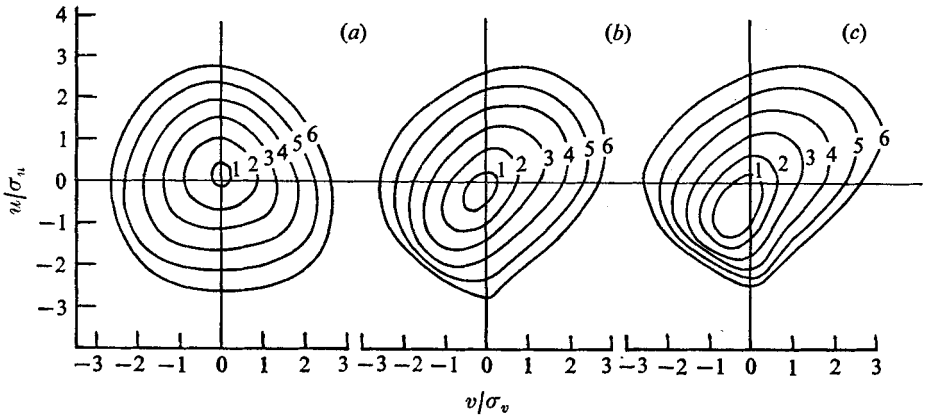

FIGURE 7. Joint probability density distributions of the u and v components of the fluctuating velocity at $x/D = 57$. Curves represent isodensity locii with the following probabilities: 1, 0·14477; 2, 0·10725; 3, 0·06505; 4, 0·03230; 5, 0·01313; 6, 0·00437. (*a*) $r/x = 0{\cdot}000$. (*b*) $r/x = 0{\cdot}056$. (*c*) $r/x = 0{\cdot}87$.

stress. A further contribution to high values of the Reynolds shear stress stems from the fact that, in the second and fourth quadrants, u and v tend to inhibit each other, contrary to the situation in the first quadrant.

3.3. *Correlation functions*

Figure 8 presents autocorrelations for u and v and the uv cross-correlation in the time domain for the radial locations $r/x = 0{\cdot}056$ and $0{\cdot}087$.

The non-dimensional function R_{uu} appears to be independent of the radial location when the time is non-dimensionalized with the integral time scale T_u,

$$T_u = \int_0^{+\infty} R_{uu}\,dt,$$

and follows closely an exponential law. As expected, an increase in r/x results in greater influence of the low frequency motions and the time during which the Eulerian co-ordinate remembers its past history also increases. No change in sign of R_{uu} was detected inside a time interval 3·5 times the integral time scale.

The independence of R_{vv} and r/x is also shown and the lower values of the integral time scale indicate that the length scales in the r direction are smaller than those in the x direction ($T_u \simeq 2{\cdot}88T_v$). The change in the sign of R_{vv} after a time interval five times the integral time scale implies the existence of a relative maximum in the high frequency region of the v spectrum.

The cross-correlation between u and v is also independent of r/x for the two locations considered but integral time scales depend on the sign of the time delay. Thus R_{uv} has not only a symmetrical component around $\tau = 0$, but also an antisymmetrical contribution implying a uv phase spectrum and a uv modulus spectrum.

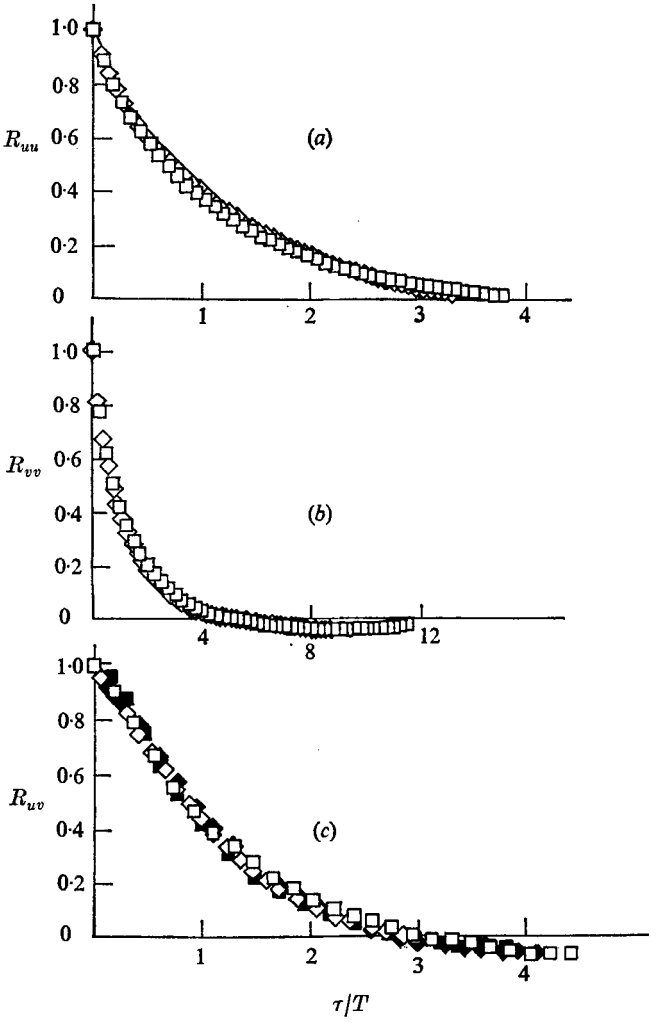

FIGURE 8. Auto- and cross-correlations of the fluctuating components u and v at $x/D = 57$. (*a*) Autocorrelation of the u component: □, $r/x = 0{\cdot}056$, $T_u = 5{\cdot}815$ ms; ◇, $r/x = 0{\cdot}087$, $T_u = 7{\cdot}217$ ms. (*b*) Autocorrelation of the v component: □, $r/x = 0{\cdot}056$, $T_v = 1{\cdot}968$ ms; ◇, $r/x = 0{\cdot}087$, $T_v = 2{\cdot}755$ ms. (*c*) Cross-correlation of u and v: □, $r/x = 0{\cdot}056$, $T_{uv} = 1{\cdot}428$ ms, u correlated with future v; ■, $r/x = 0{\cdot}056$, $T_{uv} = 1{\cdot}684$ ms, u correlated with past v; ◇, $r/x = 0{\cdot}087$, $T_{uv} = 3{\cdot}339$ ms, u correlated with future v; ◆, $r/x = 0{\cdot}087$, $T_{uv} = 2{\cdot}281$ ms, u correlated with past v.

4. Concluding remarks

Experience with the on-line digital-sampling procedure has shown it to be a convenient and precise method for quantifying the statistical characteristics of turbulent flows at least in the region of the flow where the intermittency is low. The results presented for the downstream region of a turbulent free jet provide further insight into the nature of this flow. For example, they reveal the dependence of the probability distribution of the axial velocity on the sign of

the radial velocity and, therefore, on the direction of the turbulent transport. They also quantify the deviations of the various measured distributions from Gaussian.

There is a need for further measurements of the present type but also for attempts to relate the results to design-oriented calculation methods. The present finding that the length scales are essentially constant over the non-intermittent region of the jet is consistent with Prandtl's assumption, but this is far from sufficient to characterize the other observations. Similar measurements in related but significantly different flows, for example swirling jets, will undoubtedly reveal non-constant and non-isotropic length scales; it will be interesting to determine the extent to which these can be related to the corresponding probability distributions.

The authors wish to thank Mr S. B. Pope for many useful discussions during the course of their work and Mr J. Laker for assistance with electronic components. One of the authors (M. M. R.) wishes to express his gratitude to the University of Luanda for financial support.

REFERENCES

ANTONIA, R. A. 1972 Conditionally sampled measurements near the outer edge of a turbulent boundary layer. *J. Fluid Mech.* **56**, 1.

CHAMPAGNE, F. H. & SLEICHER, C. A. 1967 Turbulence measurements with inclined hot wires. *J. Fluid Mech.* **28**, 177.

FRENKIEL, F. N. & KLEBANOFF, P. S. 1973 Probability distributions and correlations in a turbulent boundary layer. *Phys. Fluids*, **16**, 725.

GIBSON, M. M. 1963 Spectra of turbulence in a round jet. *J. Fluid Mech.* **15**, 161.

GUPTA, A. K. & KAPLAN, R. E. 1972 Statistical characteristics of Reynolds stress in a turbulent boundary layer. *Phys. Fluids*, **15**, 981.

LUMLEY, J. 1970 *Stochastic Tools in Turbulence*. Academic.

RODI, W. 1972 Ph.D. thesis, Mechanical Engineering Department, Imperial College.

WYGNANSKI, I. & FIEDLER, H. 1969 Some measurements in the self-preserving jet. *J. Fluid Mech.* **38**, 577.